



Obrabotka metallov - Metal Working and Material Science

Journal homepage: http://journals.nstu.ru/obrabotka_metallov



Electrospark deposition of chromium diboride powder on stainless steel AISI 304

Alexander Burkov^{1, a, *}, Maria Kulik^{1, b}, Alexander Belya^{1, c}, Valeria Krutikova^{2, d}

¹ Institute of Materials Science of the Khabarovsk Scientific Center of the Far-Eastern Branch of the Russian Academy of Sciences, 153 Tikhookeanskaya, Khabarovsk, 680042, Russian Federation

² Institute of Tectonics and Geophysics, Far Eastern Branch of the Russian Academy of Sciences, 65 Kim Yu Chen street, Khabarovsk, 680000, Russian Federation

^a  <https://orcid.org/0000-0002-5636-4669>,  burkovalex@mail.ru, ^b  <https://orcid.org/0000-0002-4857-1887>,  marijka80@mail.ru,

^c  <https://orcid.org/0000-0001-8795-3346>,  whitewolf-97@mail.ru, ^d  <https://orcid.org/0000-0001-9977-2809>,  nm32697@gmail.com

ARTICLE INFO

Article history:

Received: 24 February 2022

Revised: 15 March 2022

Accepted: 23 March 2022

Available online: 15 June 2022

Keywords:

Electrospark deposition

Stainless steel AISI 304

Chromium boride

Wettability

Corrosion

Oxidation resistance

Wear

Acknowledgements

Research were partially conducted at core facility "Structure, mechanical and physical properties of materials".

ABSTRACT

Introduction. Austenitic stainless steel *AISI 304* is the most widely used type of stainless steel. However, it is subject to wear due to relatively low hardness, and also begins to oxidize intensively in air at a temperature above 800 °C. The use of coatings based on chromium boride can improve its tribotechnical properties and oxidation resistance. **The purpose of the work:** to study the effect of chromium diboride concentration in the anode mixture on the structure, wear behavior, oxidation resistance and corrosion properties of electric spark coatings on *AISI 304* steel. **The research methods.** Electric spark treatment of *AISI 304* steel was carried out in a mixture of iron granules with the addition of CrB_2 powder in amount of 5, 10 and 15 vol.%. The structure of the coatings was studied by X-ray analysis, scanning electron microscopy, and electron dispersion spectroscopy analysis. The wear resistance of the coatings was studied under dry friction condition at a load of 10 N. The oxidation resistance test was carried out at a temperature of 900 °C for 100 hours. **Results and Discussion.** According to X-ray analysis, it is shown that under the conditions of electric spark exposure, CrB_2 interacts with iron melt; this has resulted in the formation of chromium and iron borides. Corrosion properties, microhardness, coefficient of friction and wear are investigated in comparison with *AISI 304* steel. Samples with coatings showed a lower corrosion potential and corrosion current density compared to the substrate in 3.5% *NaCl* solution and from 5 to 15 times higher oxidation resistance. The microhardness of the coatings increased from 6.25 to 7.60 GPa with an increase in the addition of chromium diboride in the electrode mixture. The coefficient of friction and the wear rate of all coatings were lower than that of *AISI 304* stainless steel, while the coating prepared with the addition of 5 vol.% chromium diboride had the best tribotechnical characteristics.

For citation: Burkov A.A., Kulik M.A., Belya A.V., Krutikova V.O. Electrospark deposition of chromium diboride powder on stainless steel AISI 304. *Obrabotka metallov (tehnologiya, oborudovanie, instrumenty) = Metal Working and Material Science*, 2022, vol. 24, no. 2, pp. 78–90. DOI: 10.17212/1994-6309-2022-24.2-78-90. (In Russian).

Introduction

Austenitic stainless steel *AISI 304* has excellent mechanical properties and good oxidation resistance, as well as high corrosion resistance in a wide variety of media. Because of this, *AISI 304* is the most widely used type of stainless steel and is used as structural components subject to corrosion. So it is used in the manufacture of nuclear reactors, in the medical field and in the food industry [1]. However, due to low hardness (~2 GPa), *AISI 304* steel is highly susceptible to wear [2]. The addition of carbon can increase the

* Corresponding author

Burkov Alexander A., Ph.D. (Physics and Mathematics), Senior researcher
 Institute of Materials Science of the Khabarovsk Scientific Center
 of the Far-Eastern Branch of the Russian Academy of Sciences,
 153 Tikhookeanskaya,
 680042, Khabarovsk, Russian Federation
 Tel.: 8 (914) 1618954, e-mail: burkovalex@mail.ru

hardness of stainless steel, but at the same time reduces its ductility. Application of hardening coatings can increase the surface hardness of stainless steel and improve its tribological behavior [3-4].

Cermet materials (*MC*) are a composite of ceramic phases embedded in a metal matrix [5]. Due to ceramic inclusions, *MC* coatings have a high hardness, and a plastic metal bond provides high strength and adhesion to the substrate, which together leads to high wear resistance [6-7]. Transition metal borides have high hardness and, therefore, are considered as a ceramic component of *MC* coatings [8]. Thus, it was shown in [9] that *FeCrB* coatings improve the microhardness and wear resistance of *ASTM 283-C* steel. It was shown in [10] that an increase in the content of boride ceramics in *MC* coatings leads to an increase in its microhardness. According to the paper [11], the microhardness of *AISI 304* borated steel can reach 17 GPa.

Electrospark deposition (*ESD*) is widely used to form *MC* coatings on metal base [12-14]. *ESD* is based on the phenomenon of polar metal transfer from the anode to the cathode in the process of exposure to multiple microarc discharges [15]. Due to the high cooling rate of the material, a coating with an exceptionally fine-grained structure is formed after the termination of the discharge [16]. In addition, *ESD* is characterized by high adhesion of the formed layer to the base without thermal influence on the bulk characteristics of the substrate material [17]. The modified *ESD* method with a non-localized electrode in a mixture of granules with ceramic powder has a number of advantages over traditional *ESD*, since it does not require additional operations for the preparation of *MC* electrodes and allows coating parts with a curved surface in automatic mode [18]. In addition, the method of *ESD* with a non-localized electrode is characterized by a low cost of equipment compared to other methods of deposition of *MC* coatings.

In this work to obtain *Fe-CrB* *MC* coatings, *AISI 304* stainless steel was processed in a mixture of iron granules with different concentrations of chromium diboride powder in order to establish the effect of the *CrB₂* powder concentration in the anode mixture on the structure, wear behavior, oxidation resistance and corrosion properties of the formed *ESD* coatings.

Methods

Three anode mixtures of steel granules (*St3* steel) in the form of cylinders ($d = 4 \pm 0.5$ mm, $h = 4 \pm 0.5$ mm) and *CrB₂* powder were used as a non-localized electrode (Table 1). The diameter of the powder particles was significantly smaller than the diameter of the area affected by the discharge ~ 0.8 mm, and was in the range from 25 to 134 μm with a median of 62 μm (Fig. 1). The substrate (cathode) of stainless steel *AISI 304* (Table 2) was made in the form of a cylinder ($d = 12$ mm, $h = 10$ mm). The layout of the installation for the deposition of coatings with a non-localized anode with the addition of powder is described in detail in [19]. The *IMES-40* discharge pulse source generated rectangular current pulses with amplitude of 110 A, duration of 100 μs , and frequency of 1000 Hz at voltage of 30 V. To prevent oxidation of the samples surface the argon was supplied to the working volume of the container with rate of 10 L/min.

The mass transfer kinetics was studied by successively weighing the cathode every 120 s of *ESA* on a *Vibra HT120* analytical balance with an accuracy of 0.1 mg. The total processing time for one sample

Table 1

The content of *CrB₂* in the anode mixture, designation and characteristics of coatings

<i>CrB₂</i> concentration, vol.%	5	10	15
Designation of samples	<i>Cr5</i>	<i>Cr10</i>	<i>Cr15</i>
Coating characteristics			
Thickness, μm	35.7 \pm 2.3	33.5 \pm 5.7	30.7 \pm 6.1
Roughness (Ra), μm	7.1 \pm 0.88	7.4 \pm 1.14	9.1 \pm 0.60
Water contact angle, $^\circ$	70.2 \pm 8.6	58.1 \pm 5.8	57.6 \pm 10.6

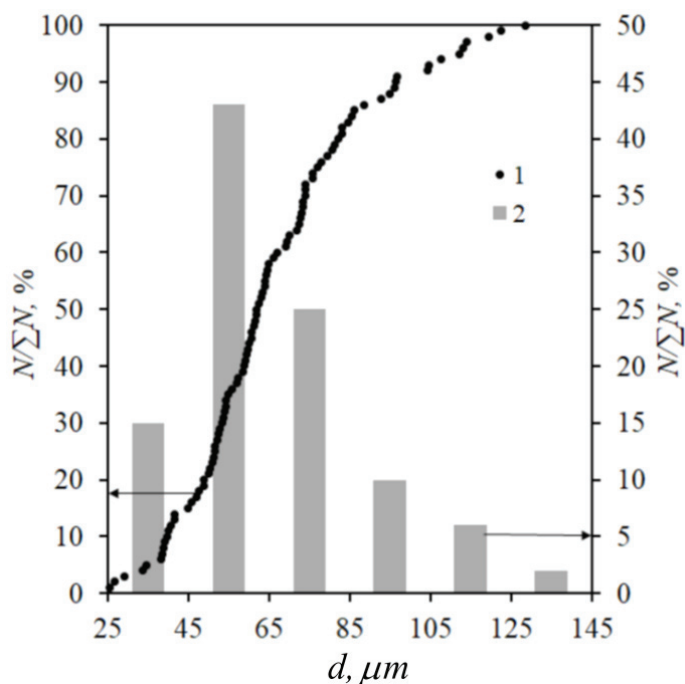


Fig. 1. Distribution of chromium diboride powder particles by diameter:
1 – integral; 2 – differential

Table 2

Chemical composition of AISI 304 steel

Element	Fe	Cr	Ni	Mn	Cu	P	C	S
Concentration, wt. %	66.3–74	18	8	≤ 2	≤ 1	≤ 0.045	≤ 0.03	≤ 0.03

was 600 s. To ensure reproducibility of the results the cathode weight gain was studied for three samples from each series. The structure of the formed coatings was studied using a *Sigma 300 VP* scanning electron microscope (*SEM*) equipped with an *INCA* Energy dispersive spectroscopy (*EDS*) analyzer and a *DRON-7* X-ray diffractometer in *Cu-Kα* radiation. The roughness of the coatings was measured on a *TR 200* profilometer. The contact angle of wetting with water was measured at room temperature according to the sessile drop method [20]. Polarization tests were carried out in a three-electrode cell in a 3.5% *NaCl* solution using a *P-2X* galvanostat (Electro Chemical Instruments, Russia) with a scanning rate of 10 mV/s. A standard *Ag/AgCl* electrode served as a reference electrode, and a paired *ETP-02* platinum electrode was used as a counter electrode. Before recording the samples were held for 30 minutes to stabilize the current of open circuit potential. Cyclic oxidation resistance tests were carried out in a muffle furnace at a temperature of 900 °C in air. Cube samples with an edge of 6 mm were kept at a given temperature for ~6 hours, then removed and cooled in a desiccator to room temperature. The total testing time was 100 hours. During the oxidation resistance test, the samples were placed in ceramic crucibles to take into account the mass of exfoliated oxides. The change in the weight of the samples was measured using a laboratory balance with a sensitivity of 10⁻⁴ g. The weight gain Δm for steel *AISI 304* and coatings after the oxidation resistance test was calculated by formula:

$$\Delta m = \frac{\Delta w}{S},$$

where Δw – weight gain and *S* – sample area.

The hardness of the coatings was measured on a *PMT-3M* microhardness tester at a load of 0.5 N using the Vickers method. The wear resistance and coefficient of friction of the samples were tested following the *ASTM G99-17* procedure under dry friction condition with speed of 0.47 ms^{-1} under load of 25 N. The testing time was 20 minutes. Discs made of *M45* high-speed steel with a hardness of 60 HRC were used as a counterbody. Wear was measured gravimetrically. The sample of each type was tested three times.

Results and discussion

The study of mass transfer during *ESD* is important for establishing the fact of a positive weight gain of the cathode, otherwise *ESD* is not effective. In addition, the coating thickness is a function of the cathode weight gain [21]. During the *ESD*, electric discharges arose between steel granules and the substrate, which resulted in a liquid-phase transfer of the metal from the granules surface to the substrate. The powder particles that appeared on the surface of the electrodes at the moment of development of the discharge channel were fused with the metal. This was accompanied by a monotonous increase in the weight gain of the cathode (Fig. 2, *a*). With an increase in the processing time for all mixtures, a slowdown in the weight gain of the cathode was observed, which is also characteristic of the traditional *ESD* [22]. This is explained by the accumulation of defects in the coating and the intensification of its electrical erosion with an increase in the specific number of discharges [23]. The largest gain of the cathode after 600 seconds of *ESA* was observed for the anode mixture of *Cr5*, and in the case of mixtures of *Cr10* and *Cr15*, taking into account the error bars, the gain can be considered close. This behavior of mass transfer can be explained by the deterioration of the electrical contact and a decrease in the frequency of discharges with an increase in the powder concentration in a mixture of granules, which was previously observed for silicon powder [24]. Therefore optimal concentration of CrB_2 powder in a mixture with iron granules is about 5 vol.% from the standpoint of achieving the maximum coating thickness.

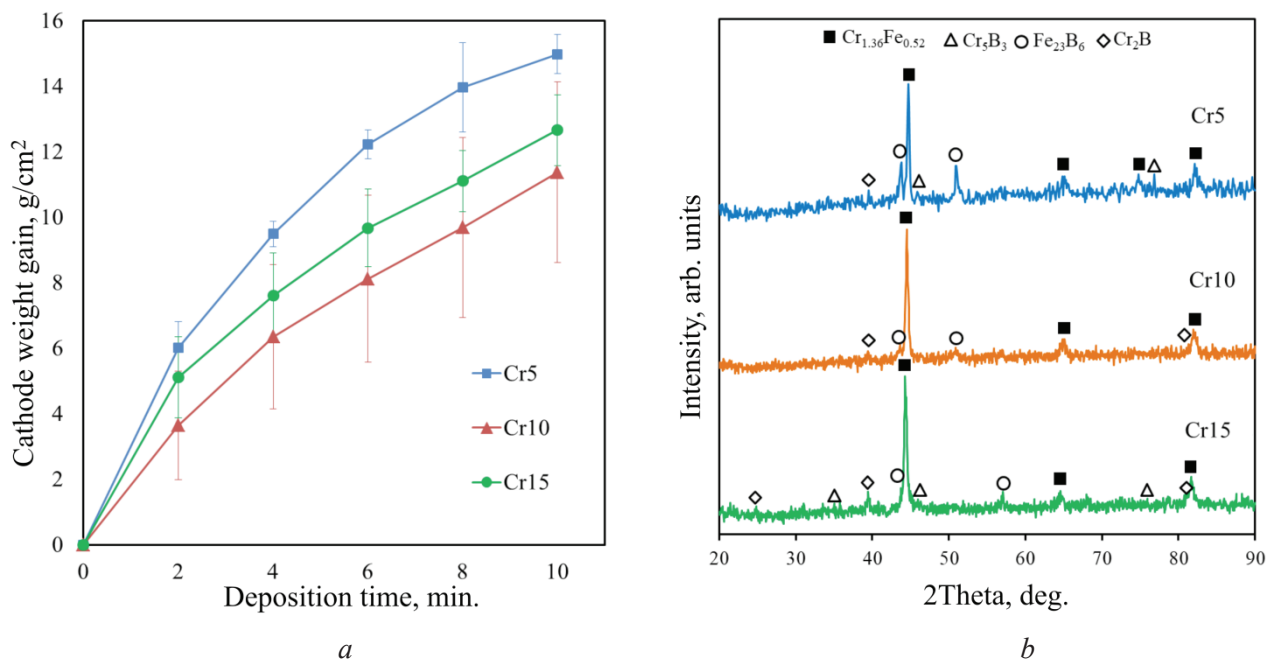


Fig. 2. AISI 304 stainless steel cathode weight gain during *ESD* (*a*) and X-ray diffraction patterns of deposited coatings (*b*)

Figure 2, *b* shows the results of X-ray analysis of the prepared coatings. From this it follows that the composition of the coatings was dominated by a solid solution of chromium in iron, which forms a metal binder of the coating, and ceramic phases of chromium (Cr_5B_3 , Cr_2B) and iron (Fe_{23}B_6) borides are also present. This indicates that the original CrB_2 phase was not retained in the coating due to its high reac-

tivity with iron and chromium melts under electric discharge conditions. Thus, in this case the mechanism of crystallization of ceramic phases from the melt after the terminated discharge is realized.

Figure 3, *a* shows a cross-sectional image of the *Cr5* coating and element distribution profile data according to *EDS* analysis. The coating has a slightly darker shade compared to the substrate due to the enrichment with boron, which was not fixed by the *EDS* analysis. Figure 3*b* shows a sharp transition between the deposited layer and the substrate. It also indicates a decrease in the concentration of substrate elements in the coating structure that is explained by the transfer of iron from the granules. The coating had a dense homogeneous structure with a small amount of small pores. With an increase in the powder concentration in the anode mixture, the average coating thickness decreased monotonically from 35.7 to 30.7 μm , and the roughness (*Ra*) increased from 7.1 to 9.1 μm (Table 1). Water contact angle (*WCA*) was measured to study the hydrophobic properties of the coating surface. The *WCA* is inversely proportional to the surface energy. As shown in Table 1, the *WCA* decreased from 70.2 to 57.6° with an increase in the concentration of CrB_2 in the anode mixture that means decrease in the hydrophobicity of its surface. However, in general electrospray *Fe-Cr-B* coatings had lower surface energy and higher hydrophobicity compared to *AISI 304* stainless steel (*WCA* 48.9°).

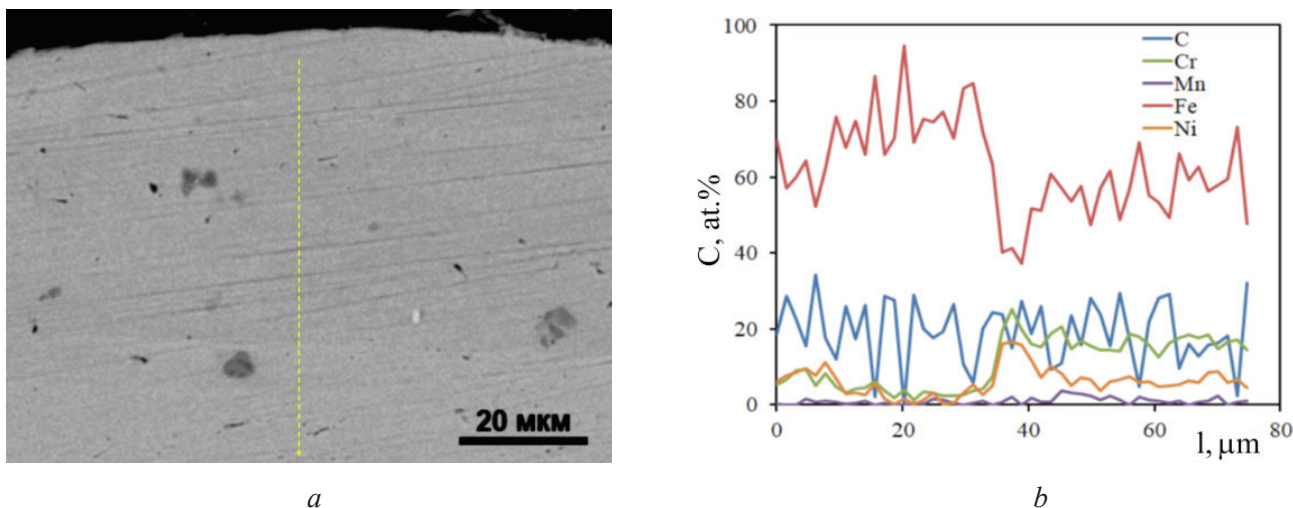


Fig. 3. SEM image of the elements of the cross-section of the *Cr5* coating in the back scattered electrons mode (*a*) and *EDS* distribution of elements in depth (*b*)

Figure 4 shows the results of polarization testing of samples in 3.5% *NaCl* solution at room temperature. It shows that the potentiodynamic curves of all coatings have significantly higher corrosion potential of E_{corr} compared to *AISI 304* steel. For detailed description of the corrosion behavior of the samples, the corrosion current I_{corr} was calculated from the slopes of the Tafel portions of the potentiodynamic curves (Table 3). It follows from Table 3 that with an increase in the amount of CrB_2 powder in a mixture of granules, the corrosion current of the coatings monotonically decreased, which indicates an improvement in the anticorrosion behavior. Thus, saturation of the *AISI 304* steel surface with chromium boride improves its anti-corrosion behavior. This is explained by the barrier action of a thin Cr_2O_3 film inevitably formed on the surface of metallic chromium [25]. In addition, ceramic phases limit the contact area of the metal with the electrolyte [6].

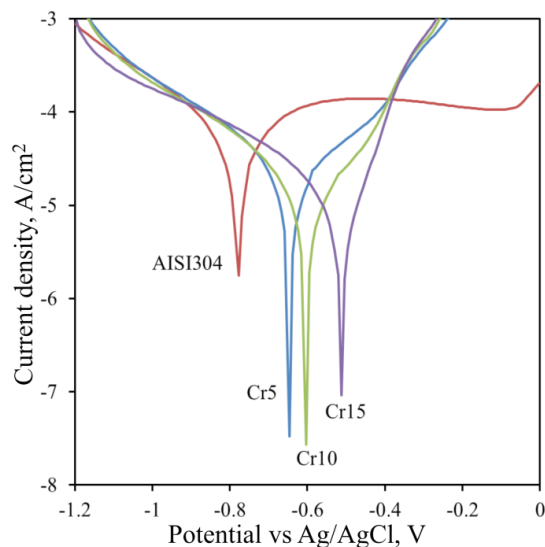


Fig. 4. Tafel polarization curves of coatings and substrate

Table 3

Corrosion parameters of coatings

Parameters	Samples			
	<i>AISI 304</i>	<i>Cr5</i>	<i>Cr10</i>	<i>Cr15</i>
E_{corr} , V	-0.777	-0.646	-0.603	-0.489
I_{corr} , $\mu\text{A}/\text{cm}^2$	42.24	20.66	14.80	11.47

Figure 5, *a* shows the results of cyclic testing of *Fe-Cr-B* coatings for oxidation resistance at a temperature of 900 °C. The weight gain of samples with coatings, according to the results of 100 hours of testing, ranged from 17 to 51 g/m². The smallest gain was observed for the *Cr15* sample, and the largest for *Cr10*, however, in this case, the weight gain is not an unambiguous criterion for the oxidation intensity. Thus, the inset to Figure 5a shows that uncoated *AISI 304* steel gained weight in the first test cycle, and monotonically substrate weight loss in subsequent cycles. This cannot be explained by the delamination of oxide layers, as was the case in [26], due to the presence of samples in ceramic crucibles during the oxidation resistance test. Therefore, the only explanation for the observed weight loss of *AISI 304* steel can be the burnout of carbon, phosphorus and sulfur included in its composition (Table 2). It is noteworthy that in the above work, for 100 hours of testing at 900 °C, the weight gain of *AISI 304* steel was only 6.5 g/m², and in [27] – 22.2 g/m² for 90 hours. The oxidation rate of the *Cr5* sample was the highest among the coatings up to 65 hours, and then the weight gain stopped, that can be explained by the action of two differently directed processes: weight loss by the substrate and weight gain of the coating. Thus, the oxidation resistance of the *Cr5* coating can be qualified as the worst. The *Cr15* coating had the best oxidation resistance. The gain in the process of high-temperature oxidation is due to the fixation of oxygen on the surface of the samples with the formation of magnetite Fe_2O_3 and hematite Fe_2O_3 (Fig. 5, *b*). According to X-ray data, ferrochrome $\text{Fe}_{0.52}\text{Cr}_{1.36}$ was also observed on the surface of the samples after the oxidation resistance test, the intensity of the reflections of which monotonically increased from the sample *Cr5* to *Cr15*. It is explained by a decrease in the thickness of the oxide layer and confirms the improvement in the oxidation resistance of coatings with an increase in CrB_2 in the anode mixture. In general, the use of electrospark *Fe-Cr-B* coatings makes it possible to increase the oxidation resistance of *AISI 304* stainless steel from 5 to 15 times.

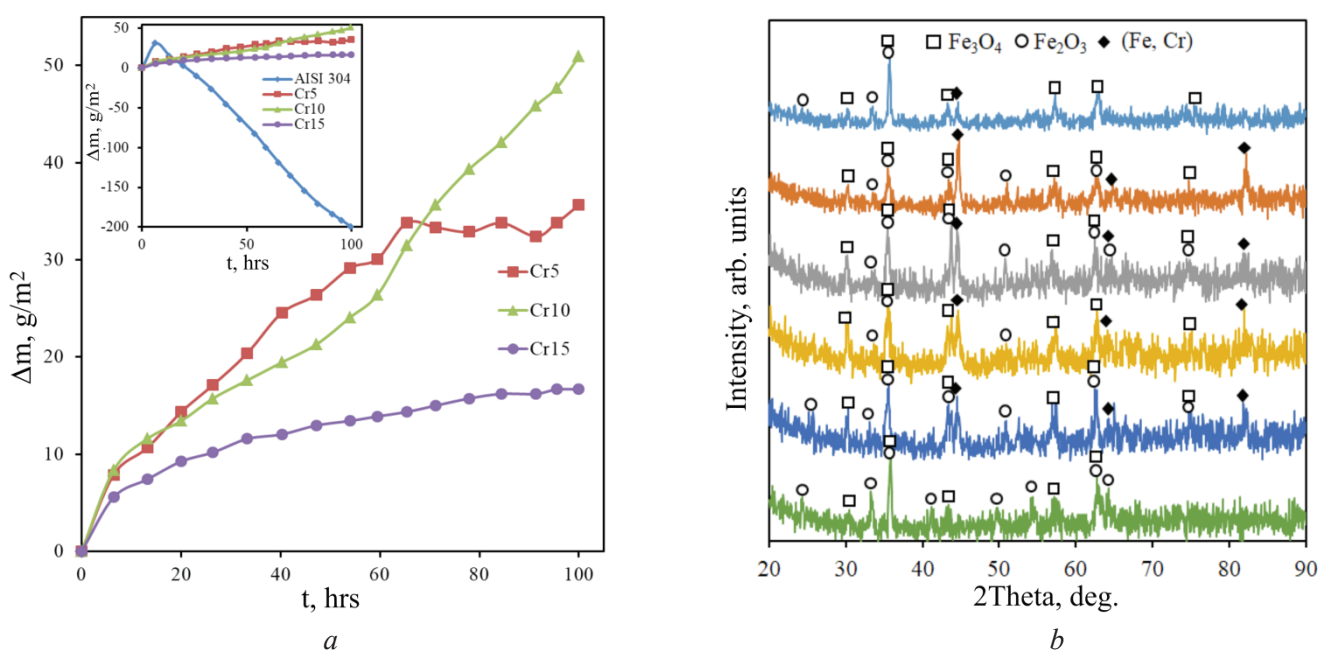


Fig. 5. Oxidation resistance of coatings at a temperature of 900 °C in air (*a*) and X-ray patterns of the samples surface after the oxidation resistance test (*b*)

Figure 6 shows that the deposition of *Fe-Cr-B* coatings makes it possible to increase the surface hardness of *AISI 304* steel by 2.2–2.7 times. With an increase in the concentration of CrB_2 powder in the anode mixture, the average microhardness of the coating surface increased from 6.25 to 7.6 GPa. This can be explained by an increase in the content of chromium and boride phases in the coating. Nevertheless, mild hardness values, compared with high hardness of borides, indicate a low volume fraction of ceramic phases in the coatings. That is consistent with the phase analysis data. In general, these results are consistent with the data obtained in [9], where the microhardness of wire-arc spraying $Fe_{87-x}Cr_{13}B_x$ coatings increased from 7.9 to 9 GPa with increase in the boron content from 1 to 4 wt.%.

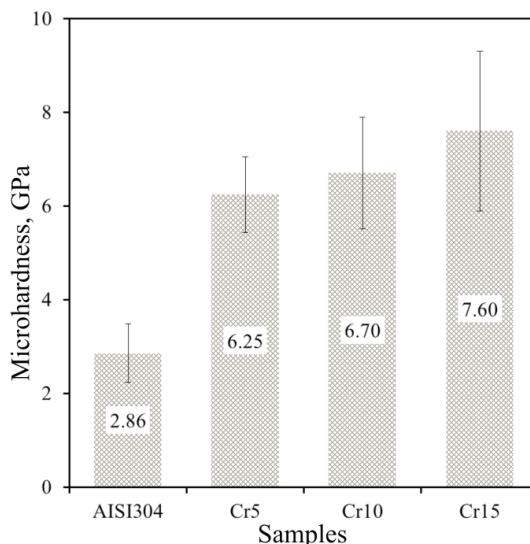


Fig. 6. Microhardness of coatings compared to *AISI 304* steel

The kinetics of the change in the coefficient of friction of the samples during the wear test under dry friction condition is shown in Figure 7, *a*. The average values of the coatings coefficient of friction were lower than those of stainless steel and were in a narrow range from 0.69 to 0.71. However, for the *Cr10* and *Cr15* samples deposited with a high powder content in the anode mixture, narrow ravines were observed in the friction coefficient curves, while the curve was smooth for the *Cr5* coating. In the case of steel, a high noise level was observed on the graph of the coefficient of friction that is usually associated with its high plasticity and with periodic deposition and delamination of the material transferred between the rubbing surfaces [28]. Thus, in particular, in samples *Cr10* and *Cr15*, noise can be caused by delamination of microsections of the coating due to deficiency of plastic metal binder.

The results of coating wear tests showed that the wear rate was in the range of $0.76\text{--}1.7 \times 10^{-5} \text{ mm}^3/\text{Nm}$ (Fig. 7, *b*). It was lower than that of *AISI 304* steel, from 1.6 to 3.7 times. The lowest wear values were demonstrated by the *Cr5* coating that is consistent with the data on the coefficient of friction. At a higher concentration of CrB_2 in the mixture of granules, the wear of the samples increased, that is caused by a de-

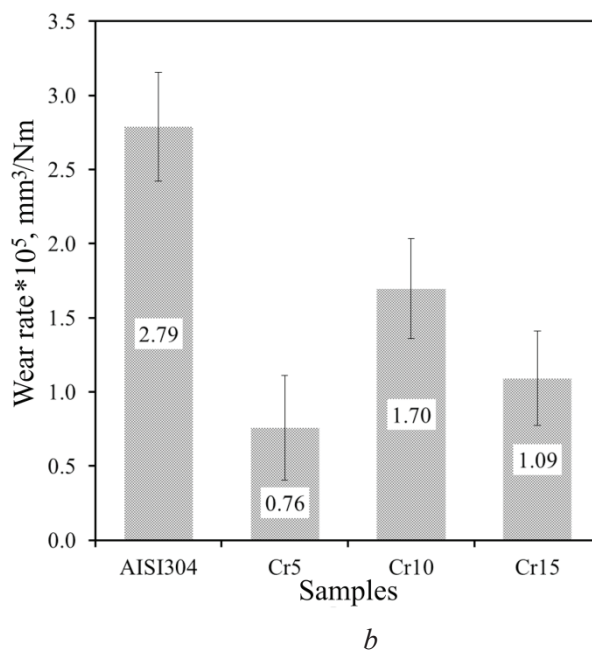
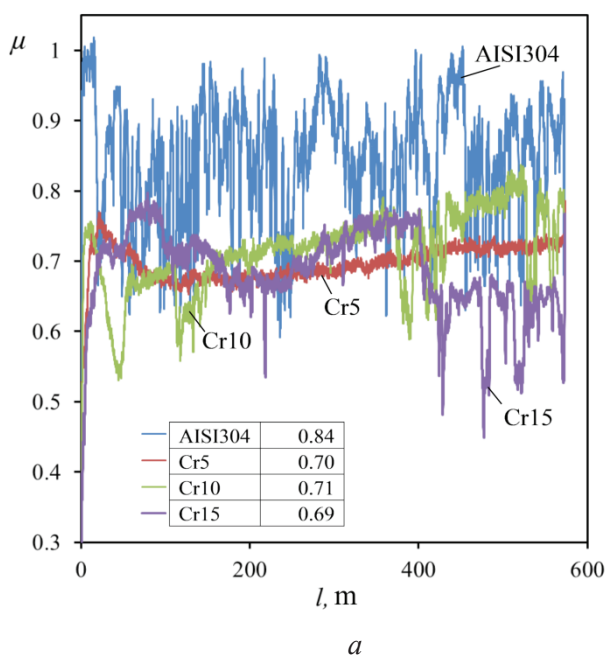


Fig. 7. Dynamics of the coefficient of friction from the sliding path (*a*) and the wear rate (*b*) of coatings compared to *AISI304* stainless steel

crease in the volume of the plastic metal binder in these coatings and increasing brittleness under friction. In addition, when analyzing the wear resistance of a *Cr5* sample, it is worth considering the large thickness of this coating compared to other samples, as indicated by the data on the cathode weight gain (Fig. 2, a).

Conclusion

Cermet *Fe-Cr-B* coatings were formed on *AISI 304* stainless steel by electrospark treatment in a mixture of iron granules and 5-15 vol.% CrB_2 powder. The largest cathode weight gain and coating thickness were in case of using an anode mixture with 5 vol.% CrB_2 . The X-ray data indicate the cermet structure of the coatings, where the role of the binder is performed by ferrochrome, and the role of ceramics are performed the Cr_5B_3 , Cr_2B , and $Fe_{23}B_6$ phases. The borides were formed as a result of the complete destruction of CrB_2 upon interaction with an iron melt under the conditions of an electric discharge. With an increase in the concentration of CrB_2 in the anode mixture, an improvement in the anticorrosion properties of *Fe-Cr-B* coatings in a 3.5% *NaCl* solution and an increase in oxidation resistance compared to *AISI 304* steel from 5 to 15 times were observed. The use of electrospark *Fe-Cr-B* coatings on *AISI 304* stainless steel makes it possible to increase its surface hardness, reduce and stabilize the friction coefficient, and improve wear resistance by 3.7 times.

References

1. Mahdavi A., Medvedovski E., Mendoza G.L., McDonald A. Corrosion resistance of boronized, aluminized, and chromized thermal diffusion-coated steels in simulated high-temperature recovery boiler conditions. *Coatings*, 2018, vol. 8, iss. 8, p. 257. DOI: 10.3390/coatings8080257.
2. Frutos A. de, Arenas M.A., Fuentes G.G., Rodríguez R.J., Martínez R., Avelar-Batista J.C., Damborenea J.J. de. Tribocorrosion behaviour of duplex surface treated *AISI 304* stainless steel. *Surface and Coatings Technology*, 2010, vol. 204, iss. 9–10, pp. 1623–1630. DOI: 10.1016/j.surfcoat.2009.10.039.
3. Ushashri K., Masanta M. Hard TiC coating on *AISI304* steel by laser surface engineering using pulsed Nd: YAG laser. *Materials and Manufacturing Processes*, 2015, vol. 30, iss. 6, pp. 730–735. DOI: 10.1080/10426914.2014.973593.
4. Sahoo C.K., Masanta M. Microstructure and mechanical properties of TiC-Ni coating on *AISI304* steel produced by TIG cladding process. *Journal of Materials Processing Technology*, 2017, vol. 240, pp. 126–137. DOI: 10.1016/j.jmatprotec.2016.09.018.
5. Golyshev A.A., Orishich A.M. Issledovanie vliyaniya rezhimov fokusirovki lazernogo izlucheniya na geometricheskie i mekhanicheskie svoystva metallokeramicheskikh trekov [Study of the laser radiation focusing modes effect on geometrical and mechanical properties of metal-ceramic tracks]. *Obrabotka metallov (tekhnologiya, oborudovanie, instrumenty) = Metal Working and Materials Science*, 2019, vol. 21, no. 1, pp. 82–92. DOI: 10.17212/1994-6309-2019-21.1-82-92.
6. Yan D., He J., Wu J., Qiu W., Ma J. The corrosion behaviour of a plasma spraying Al_2O_3 ceramic coating in dilute HCl solution. *Surface and Coatings Technology*, 1997, vol. 89, iss. 1–2, pp. 191–195. DOI: 10.1016/S0257-8972(96)02862-9.
7. Berger L.-M. Application of hardmetals as thermal spray coatings. *International Journal of Refractory Metals and Hard Materials*, 2015, vol. 49, pp. 350–364. DOI: 10.1016/j.ijrmhm.2014.09.029.
8. Mishigdorzhyn U.L., Sizov I.G., Polaynsky I.P. Formirovanie pokrytii na osnove bora i alyuminiya na poverkhnosti uglerodistykh stalei elektronno-luchevym legirovaniem [Formation of coatings based on boron and aluminum on the surface of carbon steels by electron beam alloying]. *Obrabotka metallov (tekhnologiya, oborudovanie, instrumenty) = Metal Working and Materials Science*, 2018, vol. 20, no. 2, pp. 87–99. DOI: 10.17212/1994-6309-2018-20.2-87-99.
9. Yao H.H., Zhou Z., Wang Y.M., He D.Y., Bobzin K., Zhao L., Öte M., Königstein T. Microstructure and properties of FeCrB alloy coatings prepared by wire-arc spraying. *Journal of Thermal Spray Technology*, 2017, vol. 26, iss. 3, pp. 483–491. DOI: 10.1007/s11666-016-0510-9.
10. Kılıç M. Microstructural characterization of Ni-based B_4C reinforced composite coating produced by tungsten inert gas method. *Archives of Metallurgy and Materials*, 2021, vol. 66 (3), pp. 917–924. DOI: 10.24425/amm.2021.136398.
11. Turkoglu T., Ay I. Investigation of mechanical, kinetic and corrosion properties of borided *AISI 304*, *AISI 420* and *AISI 430*. *Surface Engineering*, 2021, vol. 37, iss. 8, pp. 1020–1031. DOI: 10.1080/02670844.2021.1884332.



12. Nikolenko S.V., Konevtsov L.A., Chigrin P.G. Additive influence of carbon and carbides of vanadium and chrome in anodic tungsten-cobalt materials on their erosive fragility and formation of the alloyed layer at ESA of steels 35. *Materials Science Forum*. Trans Tech Publications, 2020, vol. 992, pp. 683–688. DOI: 10.4028/www.scientific.net/MSF.992.683.

13. Kudryashov A.E., Kiryukhantsev-Korneev Ph.V., Petrzhik M.I., Levashov E.A. Application of Zr-Si-B electrodes for electrospark alloying of Inconel 718 in vacuum, argon and air environment. *CIS Iron and Steel Review*, 2019, vol. 18, pp. 46–51. DOI: 10.17580/cisisr.2019.02.10.

14. Zhao H., Gao Ch., Wu X., Xu B., Lu Y., Zhu L. A novel method to fabricate composite coatings via ultrasonic-assisted electro-spark powder deposition. *Ceramics International*, 2019, vol. 45, iss. 17, pp. 22528–22537. DOI: 10.1016/j.ceramint.2019.07.279.

15. Chandrakant, Reddy N.S., Panigrahi B.B. Electro spark coating of AlCoCrFeNi high entropy alloy on AISI410 stainless steel. *Materials Letters*, 2021, vol. 304, p. 130580. DOI: 10.1016/j.matlet.2021.130580.

16. Shafyei H., Salehi M., Bahrami A. Fabrication, microstructural characterization and mechanical properties evaluation of Ti/TiB/TiB₂ composite coatings deposited on Ti6Al4V alloy by electro-spark deposition method. *Ceramics International*, 2020, vol. 46, iss. 10, pp. 15276–15284. DOI: 10.1016/j.ceramint.2020.03.068.

17. Li C., Ge P., Bi W. Thermal simulation of the single discharge for electro-spark deposition diamond wire saw. *The International Journal of Advanced Manufacturing Technology*, 2021, vol. 114, iss. 11, pp. 3597–3604. DOI: 10.1007/s00170-021-07132-0.

18. Burkov A.A. Poluchenie amorfnykh pokrytii elektroiskrovoi obrabotkoi stali 35 v smesi zheleznykh granuls CrMoWCBSi poroshkom [Production amorphous coatings by electrospark treatment of steel 1035 in a mixture of iron granules with CrMoWCBSi powder]. *Obrabotka metallov (tekhnologiya, oborudovanie, instrumenty) = Metal Working and Materials Science*, 2019, vol. 21, no. 4, pp. 19–30. DOI: 10.17212/1994-6309-2019-21.4-19-30.

19. Burkov A.A., Kulik M.A. Wear-resistant and anticorrosive coatings based on chrome carbide Cr₇C₃ obtained by electric spark deposition. *Protection of Metals and Physical Chemistry of Surfaces*, 2020, vol. 56, iss. 6, pp. 1217–1221. DOI: 10.1134/S2070205120060064.

20. Kwok D.Y., Neumann A.W. Contact angle measurement and contact angle interpretation. *Advances in Colloid and Interface Science*, 1999, vol. 81, iss. 3, pp. 167–249. DOI: 10.1016/S0001-8686(98)00087-6.

21. Jannaparaa N.I., Frangini S., Alphonsa J., Chauhan N.L., Mukherjee S. Comparative analysis of insulating properties of plasma and thermally grown alumina films on electrospark aluminide coated 9Cr steels. *Surface and Coatings Technology*, 2015, vol. 266, pp. 146–150. DOI: 10.1016/j.surfcoat.2015.02.028.

22. Khimukhin S.N., Eremina K.P., Nikolenko S.V. Obtaining of coatings from Ni-Al by electro spark deposition and surface smoothing by ultrasonic plastic deformation. *Materials Science Forum*. Trans Tech Publications, 2021, vol. 1037, pp. 473–478. DOI: 10.4028/www.scientific.net/MSF.1037.473.

23. Nikolenko S.V., Syui N.A. Investigation of coatings produced by the electrospark machining method of steel 45 with electrodes based on carbides of tungsten and titanium. *Protection of Metals and Physical Chemistry of Surfaces*, 2017, vol. 53, iss. 5, pp. 889–894. DOI: 10.1134/S207020511705015X.

24. Burkov A.A., Kulik M.A., Krutikova V.O. Characteristics of Ti-Si coatings on Ti6Al4V alloy subjected to electrospark granules deposition. *Tsvetnye metally*, 2019, no. 4, pp. 54–59. DOI: 10.17580/tsm.2019.04.07. (In Russian).

25. Xie Y.-j., Wang D., Wang M.-s., Ye W. Evaluation of three kinds of MCrAlY coatings produced by electrospark deposition. *Transactions of Nonferrous Metals Society of China*, 2016, vol. 26, iss. 6, pp. 1647–1654. DOI: 10.1016/S1003-6326(16)64274-7.

26. Ma J., Wen N., Wang R., Wang J., Zhang X. Li J., Chen Y. Effect of mullite film layers on the high-temperature oxidation resistance of AISI 304 stainless steel. *Coatings*, 2021, vol. 11, iss. 8, p. 880. DOI: 10.3390/coatings11080880.

27. Riffard F., Joannet E., Buscail H., Rolland R., Perrier S. Beneficial effect of a pre-ceramic polymer coating on the protection at 900 °C of a commercial AISI 304 stainless steel. *Oxidation of Metals*, 2017, vol. 88, iss. 1, pp. 211–220. DOI: 10.1007/s11085-016-9705-1.

28. Guangxiong C., Zhongrong Z., Kapsa P., Vincent L. Effect of surface topography on formation of squeal under reciprocating sliding. *Wear*, 2002, vol. 253, iss. 3–4, pp. 411–423. DOI: 10.1016/S0043-1648(02)00161-8.

Conflicts of Interest

The authors declare no conflict of interest.

